Functional Polyacetylenes Carrying Mesogenic and Polynuclear Aromatic Pendants: Polymer Synthesis, Hybridization with Carbon Nanotubes, Liquid Crystallinity, Light Emission, and Electrical Conductivity

Wang Zhang Yuan,[†,‡] Jacky W. Y. Lam,[‡] Xiao Yuan Shen,[†] Jing Zhi Sun,*[,†] Faisal Mahtab,[‡] Qiang Zheng,[†] and Ben Zhong Tang*[,†,‡]

Department of Polymer Science and Engineering, Key Laboratory of Macromolecular Synthesis and Functionalization of the Ministry of Education of China, Zhejiang University, Hangzhou 310027, China, and Department of Chemistry, The Hong Kong University of Science & Technology, Clear Water Bay, Kowloon, Hong Kong, China

Received November 9, 2008; Revised Manuscript Received January 12, 2009

ABSTRACT: Multifunctional polyacetylenes and their nanohybrids with liquid crystallinity, light emission, and electrical conductivity are developed in this work. New acetylene monomers containing biphenyl mesogens and polynuclear chromophores, namely 4-[3-(1-pyrenyl)propylcarbonyloxy]-4′-biphenylyl 11-(4-ethynylphenoxy)-undecanoate (**1**), 4-[3-(1-pyrenyl)propylcarbonyloxy]-4′-biphenylyl 10-undecynoate (**2**), and (9-fluorenyl)methyl-4-[(9-decynyl)-carbonyloxy]-4′-biphenylyloxycarbonylmethyl carbamate (**3**), were synthesized and transformed to their corresponding polymers (P**1**−P**3**) by the polymerization reactions catalyzed by organorhodium complexes of $Rh^+(nbd)[C_6H_5B^-(C_6H_5)_3]$ and $[Rh(diene)Cl]_2$. Whereas none of the monomers were mesomorphic, P**1** and P**2** were liquid crystalline. The pyrene pendants enabled P**1** and P**2** to function as dispersants for short (*s*)- and long (*l*)-multiwalled carbon nanotubes (MWNTs). P**1** assisted the dissolution of *s*- and *l*-MWNTs in THF, with respective solubilities as high as 723 and 625 mg/L. The resultant P**1**/*l*-MWNT hybrid maintained the smectic mesomorphism of P**1** and emitted bluish-green light in THF upon photoexcitation. The hybrid solid readily redissolved in common organic solvents and formed solid films upon solution casting. The hybrid films showed high electrical conductivity. This work demonstrates that polyacetylenes with multiple functionalities can be generated by attaching appropriate functional pendants to the conjugated polyene backbones.

Introduction

Conjugated polymers form the materials basis for the "plastics electronics" and have found an array of high-tech applications in optoelectronic devices[1] such as light-emitting diodes,[2] electrochemical cells,[3] field effect transistors,[4] lasers,[5] and photovoltaic cells.[6] The polymers enjoy the advantages of excellent macroscopic processability and mechanical strength, in comparison to their inorganic counterparts.[1] Liquid crystals can be molecularly oriented by external forces such as magnetic and electrical fields and mechanical stress[7] and are the quintessential molecular electronic materials for modern optical display technologies.[8] The melt of liquid crystals with conjugated polymers may generate new materials with advanced functional properties. Indeed, the mesomorphic conjugated polymers developed so far have been found, for example, to emit linearly[9] and circularly polarized lights[10] and have been employed to impart new features to electrochromic systems.[11] Furthermore, the aligned mesogens have endowed the polymers with high carrier-transport capability.[12]

Many research groups have worked on the development of mesomorphic conjugated polymers.[9−13] Polyacetylene is an archetypal conjugated polymer, and its substituted derivatives exhibit a variety of novel functional properties, such as luminescence, photoconductivity, optical nonlinearity, chain helicity, self-organizability, and biocompatibility.[14] We have worked on the development of liquid crystalline polyacetylenes and have gained valuable information on the structure−property relationships involved in the systems.[14,15] For example, whereas P**I** is not liquid crystalline, their counterparts P**II** and P**III** show mesomorphic properties (Chart 1).[15] This indicates that both skeleton rigidity and pendant interaction have exerted great influence on the alignment of the mesogenic units.

In the liquid crystalline polyacetylenes, the tails of the mesogenic units have generally been flexible alkyl chains or polar functional groups.[14,15] What will happen if bulky groups are attached to the alkyl tails? Will the resultant polyacetylene derivatives still be liquid crystalline? In the hope of conferring new functionalities on mesomorphic polyacetylenes and gaining more information on the structure− property relationships in the systems, we endeavored to incorporate bulky polynuclear aromatic units into mesogenic polyacetylenes.

Chart 1

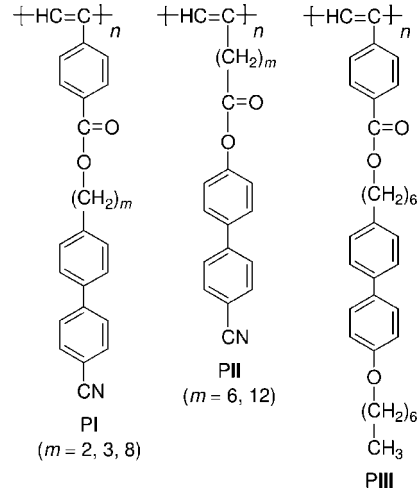

* Corresponding authors. E-mail: sunjz@zju.edu.cn (J.Z.S.); tangbenz@ust.hk (B.Z.T.).
† Zhejiang University.
‡ The Hong Kong University of Science & Technology.

10.1021/ma802510e CCC: $40.75
Published on Web 03/10/2009

Chart 2

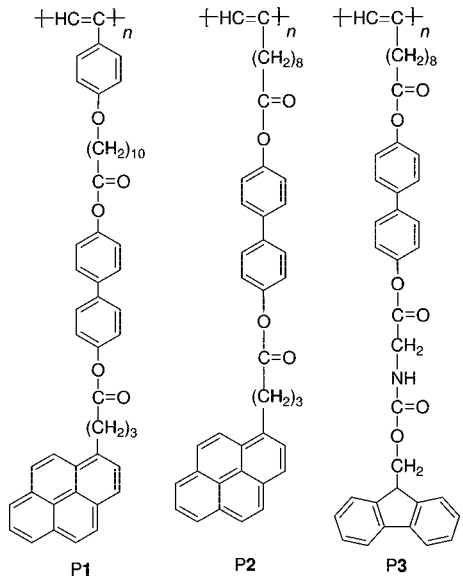

In this work, we designed and synthesized polymers P**1**−P**3**, in which pyrenyl and fluorenyl units were attached to the ends of the mesogenic pendants (Chart 2). Pyrene and fluorene rings are well-known light-emitting chromophores[16] and have been widely employed as building blocks in the construction of optoelectronic materials.[17,18] Because pyrene groups are known to readily form dimeric species in concentrated solutions and solid state,[18,19] the polymer chains of P**1** and P**2** are expected to experience strong molecular interactions. For P**3**, its amide groups can form hydrogen bonds. The formation of dimeric species and hydrogen bonds, as well as the steric effect of the bulky pendants, will inevitably affect the packing and alignment of the biphenyl mesogens in the polymers. Whether the polymers are mesomorphic or not is an open question. Delightfully, however, polymers P**1** and P**2** were found to be mesomorphic, although P**3** was not liquid crystalline.

Pyrene derivatives have often been used to help disperse carbon nanotubes (CNT) in common organic solvents.[20,21] We have been working on the creation of functional polyacetylene/CNT hybrids, with the aim of combining the merits of both components to generate new properties.[22] In this paper, we demonstrate the fabrication of processable nanohybrids of multiwalled carbon nanotubes (MWNT) and mesomorphic conjugated polymers by simply admixing MWNT with P**1** or P**2** in a common organic solvent such as THF. The P**1**/MWNT hybrid was found to exhibit liquid crystallinity, film formability, and electrical conductivity.

Experimental Section

Materials and Instruments. General information about the materials and instruments used in this work can be found in our previous paper in the series[23] and will not be repeated here in order to save the journal space. Dichloromethane (DCM) was distilled over calcium hydride under argon before use. 4,4′-Biphenol (Beijing Yangcun Chemical), 10-undecynoic acid (ABCR), Fmoc-glycine (Fluka), 1-pyrenebutyric acid (Alfa), *N*,*N*′-dicyclohexylcarbodiimide (DCC), 4-(dimethylamino)pyridine (DMAP), and *p*-toluenesulfonic acid monohydrate (TsOH; all from SCRC) were used without further purification. 11-(4-Ethynylphenoxy)undecanoic acid was prepared according to published procedures.[18] Rhodium complexes of $[Rh(cod)Cl]_2$ (cod = 1,8-cyclooctadiene), $[Rh(nbd)Cl]_2$ (nbd = 2,5-norbornadiene), and $Rh^+(nbd)[C_6H_5B^-(C_6H_5)_3]$ were prepared using literature methods.[23−25]

Melting point was measured on a MELT-TEMP II apparatus. Weight-average (M_w) and number-average (M_n) molecular weights and polydispersity indexes (PDI = M_w/M_n) of the polymers were estimated in THF by a Waters associated gel permeation chromatography (GPC) system. An Olympus BX 60 polarized optical microscope (POM) equipped with a Linkam TMS 92 hot stage was used to observe anisotropic optical textures. X-ray diffraction (XRD) patterns were recorded at room temperature on a Philips PW 1830 powder diffractometer using the monochromatized X-ray beam from the nickel-filtered Cu Kα radiation with a wavelength of 1.5406 Å (scanning rate 0.05 deg/s, scan range 2°−30°). The polymer samples for the XRD measurements were prepared by freezing the molecular arrangements in the liquid crystalline state with liquid nitrogen as reported in our previous papers.[15] Electrical conductivity of P**1** and its nanohybrid were measured on a Bio-Rad HL5500PC four-probe resistivity system.

Monomer and Polymer Syntheses. The synthetic routes to monomers **1**−**3** are shown in Schemes S1−S3 (Supporting Information). The detailed experimental procedures for the preparations of **1**−**3** and their corresponding polymers (P**1**−P**3**) as well as their spectroscopic characterization data are all given in the Supporting Information.

Polymer/CNT Hybridization. Two kinds of MWNTs, that is, short (*s*)- and long (*l*)-MWNTs with respective lengths of 0.02−1 and 1−10 μm, were used in this study. The fabrication of a hybrid of P**1**/*l*-MWNT is described below as an example. Into a tube, 15.0 mg of *l*-MWNT and 8 mL of THF were added. The *l*-MWNT was predebundled by ultrasonication for 30 min. P**1** (20.4 mg) was then added, and the resultant mixture was vigorously stirred for 1 h and homogenized by ultrasonication for 15 min. The mixture was then filtered through a cotton filter to remove the insoluble *l*-MWNT. The filter was dried in an oven at 120 °C to a constant weight. The concentration of soluble *l*-MWNT in THF (*c*) was calculated by eq 1:

$$c = \frac{W_{CNT} - (W_F - W_{F,O})}{V_S} \quad (1)$$

where W_{CNT} is the original weight of *l*-MWNT, W_F and $W_{F,0}$ are the weights of the filter after and before filtration, respectively, and V_S is the volume of the solvent. Thus, $(W_F - W_{F,0})$ is the weight of the insoluble *l*-MWNT that was retained by the filter, and $W_{CNT} - (W_F - W_{F,0})$ is the weight of the soluble *l*-MWNT that has passed through the filter.

Results and Discussion

Polymer Synthesis. Monomers **1**−**3** were synthesized by the esterification reactions using DCC as dehydrant (cf. Scheme S1−S3 in the Supporting Information). The reactions proceeded smoothly, and all the desired monomers were obtained in high yields (70−86%). $[Rh(nbd)Cl]_2$ was first used to polymerize **1** in a mixture of THF and triethylamine (TEA). The solution maintained homogeneous with no solid precipitated during the whole process of polymerization reaction. However, after precipitating in methanol and drying in a vacuum oven at 40 °C, the polymeric product became partially insoluble in THF. The GPC curve of the soluble fraction contains two separated peaks, with M_w/PDI values of 137500/3.3 and 4400/1.1 for peaks 1 and 2, respectively (Table 1). This indicates that high molecular weight polymer and low molecular weight oligomer have been produced simultaneously during the polymerization process.

In our previous work, we have found that a polymer becomes insoluble when its molecular weight goes beyond a certain value.[18a] The insolubility of part of the P**1** product may be due to its very high molecular weight. To obtain completely soluble product, the molecular weight of the polymer needs to be controlled. Fortunately, by simply changing the solvent to DCM/Et_3N, we succeeded in realizing our goal: a polymer with a moderate M_w value (93 100) was obtained, which was completely soluble in common organic solvents (Table 1, no. 2).

Table 1. Polymerization of Monomers 1−3[a]

no.	catalyst	solvent	yield (%)	M_w	PDI
		Monomer **1**			
1	$[Rh(nbd)Cl]_2$	THF/TEA	68	137 500[b]	3.3[b]
2	$[Rh(nbd)Cl]_2$	DCM/TEA	76	93 100	1.8
3	$[Rh(cod)Cl]_2$	DCM/TEA	52	83 400	1.7
		Monomer **2**			
4[c]	$[Rh(cod)Cl]_2$	dioxane/TEA	20	5 900	1.3
5[d]	$Rh^+(nbd)[C_6H_5B^-(C_6H_5)_3]$	THF	73	9 700	1.7
6	$Rh^+(nbd)[C_6H_5B^-(C_6H_5)_3]$	THF	74	16 100	1.6
		Monomer **3**			
7	$Rh^+(nbd)[C_6H_5B^-(C_6H_5)_3]$	THF	76	22 400	1.7

[a] Carried out under nitrogen at room temperature for 24 h. $[M]_0 = 0.2$ M, [cat.] = 2 mM. Abbreviations: THF = tetrahydrofuran, cod = 1,5-cyclooctadiene, nbd = 2,5-norborndiene, TEA = triethylamine, M_w = weight-average molecular weight, and PDI = polydispersity index (estimated by GPC in THF on the basis of a polystyrene calibration). [b] Soluble before precipitation but became partially soluble in THF after precipitation in methanol and dried in vacuo; data given here are for the soluble fraction with high molecular weight. [c] Carried out at 60 °C. [d] [Cat.] = 4 mM.

Similar results were obtained when $[Rh(cod)Cl]_2$ was used as catalyst.

Unlike monomer **1**, monomer **2** is a 1-alkyne derivative, whose polymerization behavior differs from that of a phenylacetylene derivative.[14,18,26] As can be seen from Table 1, when $[Rh(cod)Cl]_2$ is used as catalyst in 1,4-dioxane/TEA, only is an oligomer (M_w = 5900) obtained in a low yield (20%). It is known that the zwitterionic rhodium complex of $Rh^+(nbd)[C_6H_5B^-(C_6H_5)_3]$ is an effective catalyst for 1-alkyne polymerization.[18,26] We thus attempted to polymerize **2** in THF by $Rh^+(nbd)[C_6H_5B^-(C_6H_5)_3]$. Delightfully, at a concentration of 4 mM, the zwitterionic complex performed well, giving a polymer with a moderate molecular weight in a high yield (73%). The molecular weight of the polymer was increased (M_w = 16 100) by decreasing the catalyst concentration to 2 mM (Table 1, no. 6).

Considering the structural similarity between **3** and **2**, we used $Rh^+(nbd)[C_6H_5B^-(C_6H_5)_3]$ to catalyze the polymerization of **3**. The result was satisfactory: P**3** with an M_w of 22 400 was obtained in 76% yield (Table 1, no. 7). It should be pointed out that, when $[Rh(nbd)Cl]_2$ was used to catalyze **3** in THF/TEA at room temperature, the polymerization was sluggish, and P**3** was obtained in ∼8% yield. This proves that $[Rh(diene)Cl]_2$ is inefficient in alkyne polymerization, while $Rh^+(nbd)[C_6H_5B^-(C_6H_5)_3]$ is an excellent catalyst.

Structure Characterization. Spectroscopic methods were used to characterize the structures of the polymers. All the polymers gave satisfactory analysis data corresponding to their expected molecular structures (see Experimental Section for details). An example of the IR spectrum of P**1** is given in Figure 1; the spectrum of its monomer (**1**) is given in the same figure for comparison. The monomer exhibits absorption band at 3268, 2104, and 1754 cm^{-1}, which are due to stretching vibrations of ≡CH, C≡C, and C═O, respectively. While the C═O stretching band maintains intact, the acetylenic bands are no longer seen in the spectrum of P**1**, indicating that the triple bond of **1** has been consumed by the polymerization reaction.

Figure 2 shows the ^1H NMR spectra of **1** and P**1**. There is no peak at $\delta \sim 2.99$ in the spectrum of P**1**, which is associated with the resonance of acetylene proton. A new peak due to the resonance of the olefinic protons appears at $\delta \sim 5.80$ in the spectrum of P**1**, which is absent in the spectrum of **1**. This proves that the acetylenic triple bond of **1** has been transformed to the olefinic double bond by the polymerization reaction. The acetylene polymerization shifts the resonance peaks of phenyl protons from $\delta \sim 7.40$ and 6.81 in **1** to $\delta \sim 6.51$ in P**1** (cf. peaks b and c in panels A and B of Figure 2). This is due to the electron-rich nature of the polyacetylene backbone, which exerts a powerful shielding effect on the neighboring aromatic protons. All other resonance peaks can be readily assigned with no unexpected signals found, as can be clearly seen from Figure 2.

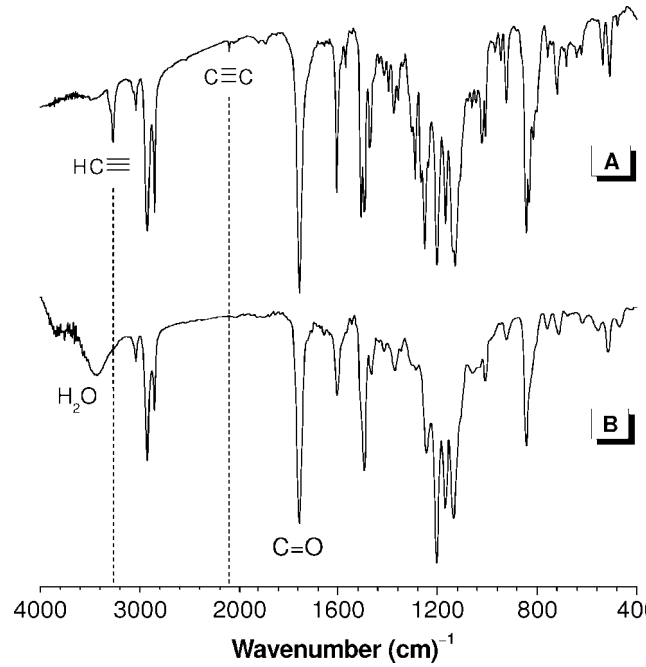

Figure 1. IR spectra of (A) **1** and (B) its polymer P**1** (sample from Table 1, no. 2).

Figure 3 shows the ^{13}C NMR spectra of P**1** and its monomer **1**. Whereas the acetylenic carbon atoms of monomer **1** resonate at δ 76.5 (≡CAr) and 83.7 (HC≡), these peaks are completely absent in the spectrum of P**1**. The polyene backbone resonances, however, are hard to distinguish due to their overlap with the carbon resonances of the aromatic pendants, namely, phenyl, biphenyl, and pyrenyl groups. The result agrees well with the IR and ^1H NMR analyses, thus duly verifying the successful synthesis of P**1**.

Polymer/CNT Hybridization. In our previous studies, we have found that PPA and its derivatives are superior to their monomers or nonconjugated polymer counterparts in terms of dispersing CNT in organic solvents.[18,22] PPA can be used to functionalize CNT through noncovalent interaction, which has the advantage of not perturbing the electronic structure of CNT. It is well-known that planar aryl rings, such as pyrene[20,21] and porphyrin,[27] readily form complexes with the CNT surfaces via strong $\pi-\pi$ interaction. Our polymers are expected to show strong solvating power to CNT. Hybridizations of P**1** and P**2** with *s*- and *l*-MWNTs were thus investigated.

As expected, under all the tested conditions, soluble polymer−CNT nanohybrids were obtained. For *s*-MWNT, no matter whether P**1** or P**2** was used, highly soluble nanohybrids were always obtained. The resultant nanohybrid solutions show

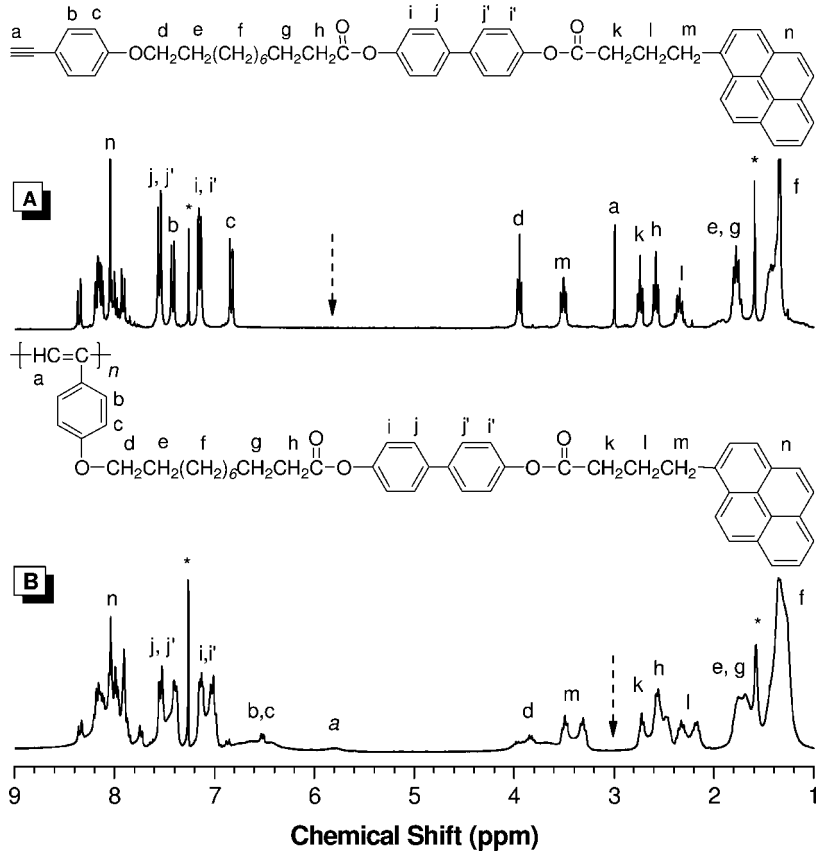

Figure 2. [1]H NMR spectra of (A) **1** and (B) its polymer P**1** (sample taken from Table 1, no. 2) in chloroform-*d* at room temperature. The solvent peaks are marked with asterisks.

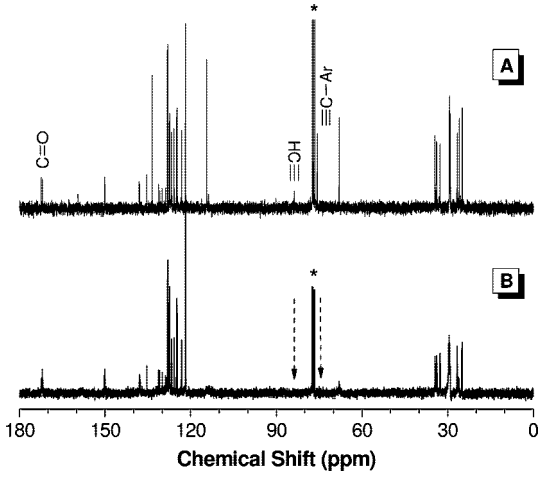

Figure 3. [13]C NMR spectra of (A) **1** and (B) its polymer P**1** (sample taken from Table 1, no. 2) in chloroform-*d* at room temperature. The solvent peaks are marked with asterisks.

long-term stability and maintain homogeneous for 1 month without precipitation. However, for *l*-MWNT, although both P**1** and P**2** are good dispersants, the long-term stability of their hybrids differs from each other: the P**1**/*l*-MWNT solution can keep homogeneous for weeks, whereas the P**2**/*l*-MWNT solution becomes inhomogeneous after standing for a couple of days. The results indicate that P**1** is a better dispersant than P**2**. The difference in the solvating power between P**1** and P**2** may be ascribed to the difference in their backbone structure: the PPA skeleton of P**1** can readily wrap onto the MWNT walls,[22a] whereas the poly(1-alkyne) skeleton is less affinitive to the MWNT surfaces.[18b]

Both P**1** and P**2** are better hybridized with *s*-MWNT than *l*-MWNT, as manifested by the higher solubility and better long-term stability of the polymer/*s*-MWNT hybrids in THF. The lower solubility of *l*-MWNT is understandable because it is more difficult to debundle *l*-MWNT than *s*-MWNT. Even after debundling, *l*-MWNT strands have higher tendency to entangle together to form new agglomerates. It also has much higher strand weight than that of *s*-MWNT and is therefore easier to precipitate from the solvent after functionalization. The long-term stability of its hybrids is thus not as good as that of the *s*-MWNT hybrids.

Morphological Structures. The solvating power of P**1** and P**2** to CNT stems from the π-electronic interactions between the polymer chains and the CNT surfaces. To "see" how these two components interact with each other, transmission electron microscope (TEM) measurements of the nanohybrids were carried out. As can be seen from panels A and B of Figure 4, the polymer chains form coating layers on *s*-MWNT with thickness of ~20−30 nm. Interestingly, P**1** chains wrap around the *l*-MWNT surfaces to form thin polymer coating as well as a unique "pearls on a string" structure (Figure 4C). The P**2**/*l*-MWNT hybrid, however, have a normal core/shell structure. The effective coating proves good adherence of the polymer chains to the CNT walls and strong interactions between the polymer chains.

To further examine the wrapping or coating of the polymer chains around the MWNT walls, hybrid films were fabricated on glass substrates from THF solutions of P**1**/*l*-MWNT. As can be seen from the scanning electron microscope (SEM) image of the hybrid film shown in Figure 5A, the P**1** chains and the *l*-MWNT wires form an interpenetrating networklike structure. It also manifests the high loading of *l*-MWNT in the nanohybrid. Figure 5B shows a magnified image of a selected area in Figure

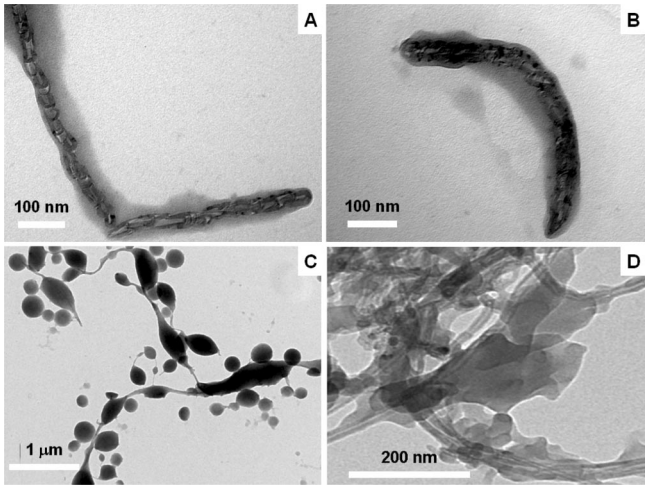

Figure 4. TEM images of the hybrids of polyacetylenes with short (*s*) and long (*l*) multiwalled carbon nanotubes (MWNT): (A) P**1**/*s*-MWNT, (B) P**2**/*s*-MWNT, (C) P**1**/*l*-MWNT, and (D) P**2**/*l*-MWNT. The samples were prepared from their diluted THF solutions.

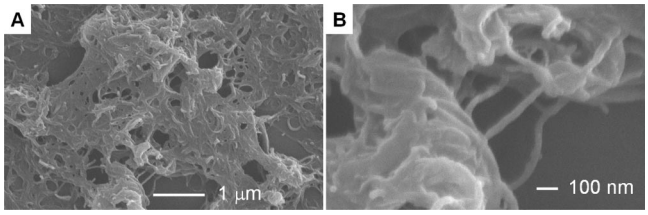

Figure 5. SEM images of P**1**/*l*-MWNT hybrid.

Chart 3

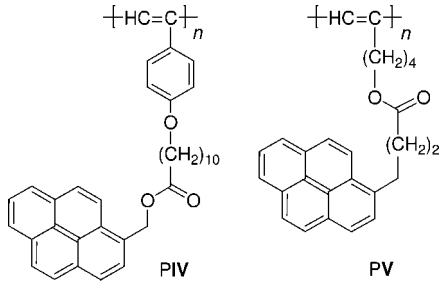

5A. Evidently, the wrapped *l*-MWNT wires are partially embedded in the polymer matrix. These SEM images again testify the strong interaction between the polymers and MWNTs.

Solvating Power. As mentioned above, both P**1** and P**2** show strong solvating power toward CNT. Monomers **1** and **2** are also good dispersants for CNT, thanks to their pyrenyl and biphenyl groups. To quantitatively evaluate the solvating power, we measured the solubility of the MWNT functionalized by different dispersants under the same conditions as previously reported for P**IV** (Chart 3).[18] In a typical test, predetermined amounts of polymer (0.0275 mmol) and MWNT (15 mg) were mixed with a specific volume of THF (8 mL) to make sure that the data can be comparable with each other.

Figure 6 depicts the solubilities of the *s*- and *l*-MWNTs hybridized with the monomers and polymers. Although **1** and **2** can be used as dispersants for CNT, their solvating capacities are limited: for example, the solvating powers of **1** and **2** toward *l*-MWNT are 100 and 75 mg/L, respectively. The solubility of *s*-MWNT in THF is somewhat higher than that of *l*-MWNT under the same conditions. Thanks to the "polymer effect",[18b,22c] when **1** and **2** are replaced by their polymers P**1** and P**2**, the solvating powers are dramatically improved. For *l*-MWNT, the

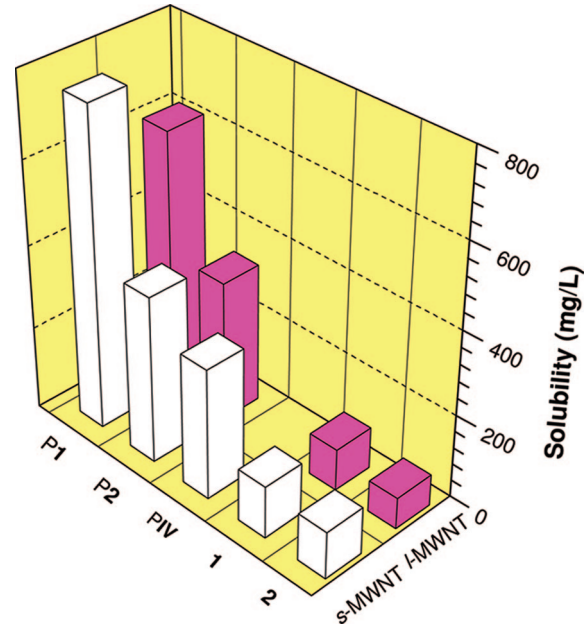

Figure 6. Solubilities of the *s*- and *l*-MWNTs hybridized with **1**, **2**, P**1**, and P**2** in THF. Data for P**IV** are shown for comparison.

solvating powers of P**1** and P**2** are 625 and 338 mg/L, respectively, which are more than 6- and 4-fold higher than those of the monomers. The results are even better for *s*-MWNT: its hybrids with P**1** and P**2** show solubility in THF as high as 763 and 400 mg/L, respectively.

Close examination of the solubility data reveals that P**1** always shows stronger solvating power than P**2**, no matter whether *s*- or *l*-MWNT is used. The solvating power of a dispersant strongly depends on its molecular structure. The major structural difference between P**1** and P**2** lies in the polymer skeleton. Evidently, with the same pendant group, the PPA derivative serves as a better dispersant for MWNT, in comparison to its poly(1-alkyne) counterpart. This is reasonable because the PPA skeleton can wrap onto the MWNT surfaces,[22a] whereas the olefinic main chain of poly(1-alkyne) makes little contribution to the dispersion of MWNT in solvents.[18b] Thus, in the P**1**/MWNT system, both "polymer wrapping" and "pendant complexation" processes contribute to the MWNT dispersion, whereas in the P**2**/MWNT hybridization process, only "pendant complexation" is at work.

We also compared the solvating power of P**1** with that of P**IV**, which is a congener of P**1** without the biphenyl unit in the pendant group. As can be seen from Figure 6, the solubility of the *s*-MWNT hybridized with P**IV** is only 313 mg/L,[18a] much lower than that of the *s*-MWNT hybridized with P**1**. The result suggests that the biphenyl unit exerts a synergistic or cooperative effect on the solvating power of the polymer or the dissolution of the MWNT.

Thermal Stability. Notwithstanding the excellent conductivity of its doped form, polyacetylene has found few technological applications owing to its notorious intractability and instability. Substituted polyacetylenes generally show better processability and higher stability over its polyacetylene parent. However, PPA shows a decomposition temperature (T_d, defined as the temperature at which a polymer loses 5% of its original weight) of 225 °C;[28] that is, the polymer becomes unstable when thermally treated. Disubstituted polyacetylenes are thermally stable due to the total replacement of the hydrogen atoms in the polyene backbone by aromatic or alkyl groups. For example, the T_d value for poly(1-phenyl-1-propyne) is 330 °C,[28,29] which is comparable to that of polystyrene (330 °C),[30] a stable commodity polymer. Although

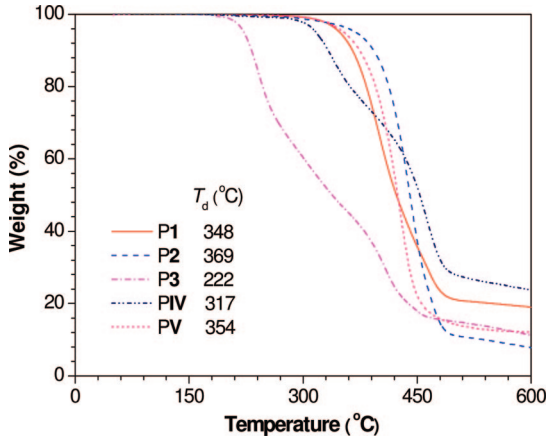

Figure 7. TGA thermograms of P**1** (sample from Table 1, no. 2), P**2** (Table 1, no. 5), P**3** (Table 1, no. 7), P**IV**, and P**V** measured under nitrogen at a heating rate of 10 °C/min.

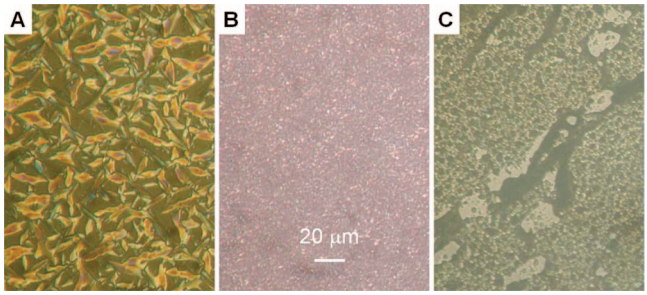

Figure 8. Mesomorphic textures observed on cooling (A) P**1** to 150 °C, (B) P**2** to 165 °C, and (C) P**1**/*l*-MWNT to 150 °C from their isotropic states at a cooling rate of 3 °C/min.

the existence of hydrogen atoms in the backbones of monosubstituted polyacetylenes is not in favor of their stabilities, it is found that bulky pendants can greatly enhance their thermal resistances. For example, P**IV** and P**V** are thermally stable: their T_d values are as high as 317 and 354 °C, respectively (Figure 7), thanks to their very bulky pyrene pendants.

The thermal stabilities of P**1** and P**2** are remarkably high, noting that they are monosubstituted polyacetylenes. As shown in Figure 7, the T_d values of P**1** and P**2** are 348 and 369 °C, respectively, which are even higher than those of polystyrene and poly(1-phenyl-1-propyne). The high stability is evidently due to the incorporation of the biphenyl and pyrenyl pendants into the polymer structures. This testifies the "jacket effect" of bulky pendants on the thermal stability of polyacetylenes.[14,15,18,31] From the comparison of the TGA data of P**1** and P**2** with those of P**IV** and P**V**, the improvements in T_d values are 31 and 15 °C, respectively. From their chemical structures, it is easy to find out that the introduction of the biphenyl units has contributed to the thermal stability of the polymers. However, although both biphenyl and fluorenyl pendants have been incorporated into the structure of P**3**, its T_d value is low (222 °C), probably due to the easy cleavage of the fluorenyl groups by thermolysis.

Liquid Crystallinity. After checking the thermal stabilities of the polymers, we proceeded to study their mesomorphic behaviors. Figure 8 shows the POM microphotographs of the textures of P**1**, P**2**, and P**1**/*l*-MWNT recorded in the heating−cooling cycles. When P**1** was cooled from its isotropic state, small bâtonnets emerged from the homotropic dark background, forming an anisotropic mesomorphic texture. This indicates that P**1** is liquid crystalline. The texture contains tiny bands, whose directors are perpendicular to the long axes of the bâtonnets. Such in-domain bands have often been observed during the formation of the

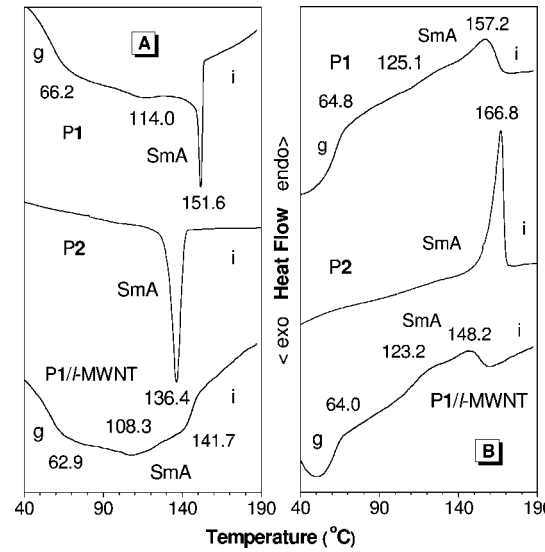

Figure 9. DSC thermograms of P**1** (Table 1, no. 2), P**2** (Table 1, no. 5), and P**1**/MWNTs recorded under nitrogen during the (A) first cooling and (B) second heating scans at a scan rate of 10 °C/min.

focal-conic textures in liquid crystalline polyacetylenes,[15a,31a,32] suggesting that the mesophase of P**1** is smectic A in nature. Our attempt to grow the bâtonnets to bigger focal-conic domains failed. This is probably because the rigid PPA skeleton and the strong $\pi-\pi$ interaction between the pyrenyl groups have prevented the texture from further developing.

When P**2** was cooled from its melt state, many anisotropic entities emerged from the background (Figure 8B). However, the development of these tiny entities into a typical SmA texture was difficult. For P**3**, the POM observation gave a disappointing result that it was not liquid crystalline. This is probably due to the hydrogen bonds between the amide groups and steric effect of the fluorenyl units. It is worth pointing out that none of the monomers show mesomorphic textures. Thus, although **1** and **2** are nonmesomorphic, their polymers P**1** and P**2** are liquid crystalline. This indicates that the polymer chain plays an active role in the alignment and packing of the mesogenic pendants.

Encouraged by our success of obtaining pyrene-containing liquid crystalline polyacetylenes, we continued to examine whether their hybrids with CNT are mesogenic. The P**1**/*l*-MWNT hybrid was selected as an example to check. As shown in Figure 8C, small-size grains are visible in the microphotograph. It indicates that the hybrid is mesomorphic, although the alignment and packing of the mesogens in the hybrid are worse than those in the pure polymer. This is reasonable, since *l*-MWNT can be regarded as an "impurity" in huge size, which hampers the growth of the anisotropic domains.

Differential scanning calorimetry (DSC) measurements were carried out to evaluate the thermal transition temperatures. Figure 9 shows the DSC thermograms of P**1** and P**2** recorded under nitrogen during the first cooling and second heating scans. In the first cooling circle, P**1** enters the SmA phase from its isotropic state at 151.6 °C. The mesophase is stable in a temperature range over 37 °C before the polymer solidifies at 114.0 °C. The associated g-SmA and SmA-i transitions are observed at 125.1 and 157.2 °C, respectively. The transition profiles of P**2** are somewhat different from those of P**1**. In its first cooling circle, a broad exothermic peak associated with i-SmA is observed at 136.4 °C and the corresponding SmA-i transition is detected at 166.8 °C.

To find out the effect of CNT on the thermal transitions, we run the test on the P**1**/*l*-MWNT hybrid. As can be seen from Figure 9, its transition profiles are similar to those of P**1** and the i-SmA and SmA-g transitions are found at 141.7 and 108.3

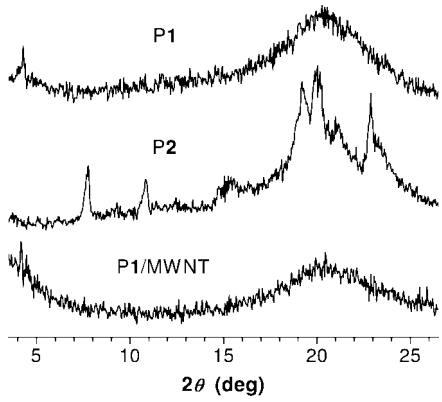

Figure 10. XRD patterns of liquid crystalline samples of P**1** (sample from Table 1, no. 1), P**2** (Table 1, no. 5), and P**1**//*l*-MWNT. The samples were heated to 190 °C, cooled to 130 °C at a rate of 3 °C/min, and then kept at 130 °C for 30 min before being rapidly quenched by liquid nitrogen.

°C, respectively. The peaks corresponding to the SmA-i and g-SmA transitions are observed at 123.2 and 148.2 °C, respectively. The data indicate that the transition temperatures of the nanohybrid are lower than those of its pure polymer parent. The incorporation of *l*-MWNT distorts the alignment of the polymer chains, and the resultant loose stacking or packing decreases the transition temperatures.

To verify the mesophase assignment and to learn more about the molecular packing arrangements, XRD analyses were conducted. The diffractogram of a powder sample can be generally divided into the low-angle Bragg reflections at $2\theta \sim 3°$ corresponding to the layer spacing of molecular orientational order and the high-angle peaks at $2\theta \sim 20°$ associated with the liquidlike intermesogenic organization within the layers.[33] The appearance of a broad or sharp peak serves as a qualitative indication of the degree of order. As can be seen from Figure 10, P**1** shows an XRD pattern consisting of low- and high-angle peaks. The diffuse peak centered at $2\theta = 20.39°$ gives an average distance (d_2) of 4.35 Å (Table 2) associated with the lateral packing arrangement of the pendants. In the low-angle region, it gives a Bragg reflection at $2\theta = 4.28°$. The layer thickness is calculated to be 20.62 Å, which is shorter than the fully extended molecular length of the monomer unit ($l = 38.09$ Å) but close to that of the terminal unit containing the biphenyl and pyrenyl groups (23.51 Å; Chart 4).

Different from P**1**, P**2** exhibits two peaks in the low-angle region and several peaks in the high-angle region. The layer spacing (d_1) of 11.38 Å derived from the Bragg reflection at $2\theta = 7.76°$ is close to the length of the biphenyl mesogenic unit, suggesting that the pyrenyl group is not participating in the mesogenic packing arrangement in this polymer. This is supported by the sharper peaks in the high-angle region, which may be associated the separate packing of the pyrenyl groups. The P**1**//*l*-MWNT hybrid shows two peaks almost identical to those of P**1**. However, because of the presence of *l*-MWNT, the packing order of the mesogens is worsened, as reflected by the weaker intensity of the low-angle peak. The result is consistent with the POM observation: the MWNT does not destroy the liquid crystallinity of P**1** but disturbs the alignment of its mesogenic pendants.

Light Emission. Monosubstituted polyacetylenes, particularly PPA derivatives, generally luminesce weakly.[34] However, when emissive pendants are properly introduced, monosubstituted polyacetylenes can become emissive.[18,22e,35] Pyrene is a famous emissive chromophore. By incorporating it into the polymers, luminescent P**1** and P**2** are obtained. Figure 11 shows the photoluminescence (PL) spectra of P**1** and P**2**. The PL spectra of **1**, **2**, P**1**//*l*-MWNT and P**2**//*l*-MWNT are also given in the same figure for the purpose of comparison. The dilute THF solutions of **1** and **2** exhibit the "monomer" emission of pyrene at 377 and 397 nm upon photoexcitation. However, their polymers P**1** and P**2** show the "monomer" emission as well as the "excimer" emission at 475 nm, even at very low concentrations. This indicates that the adjacent pyrene pendants in the polymer chain experience strong intramolecular interactions, which facilitate the excimer formation. The ratios of the intensities of the monomer (I_M) and excimer (I_E) emissions for P**1** and P**2** are 1:0.95 and 1:6.1, respectively. This suggests that the poly(1-alkyne) skeleton enable ready aggregation of the pyrene chromophores.

P**1**//*l*-MWNT and P**2**//*l*-MWNT hybrids emit in similar manners to their polymer parents. As can be seen from Figure 11, their PL spectral profiles are virtually identical. To collect further information about the effect of the CNT on the light emission, fluorescence quantum yield (Φ_F) was measured using 9,10-diphenylanthracene as standard ($\Phi_F = 90\%$ in cyclohexane). Because P**1**, P**2**, P**1**//*l*-MWNT, and P**2**//*l*-MWNT have similar absorption feature (Figure S5), an excitation wavelength of 343 nm was used for the PL spectrum measurement. It is worth noting that the Φ_F value of P**2** (11.2%) is much higher than that of P**1** (4.2%). This is because the PPA skeleton can effectively quench the PL of P**1**.[34]

The introduction of MWNT into a fluorescence system usually quenches the light emission. As can be seen from Figure 11B, the Φ_F value of P**2**//*l*-MWNT is 6.5%, which is much lower than that of P**2** (11.2%). The Φ_F value of P**1**//*l*-MWNT (4.5%), however, is not decreased but slightly increased, in comparison with that of P**1** (4.2%; Figure 11A). These data are consistent with our previous results, where fluorescence quenching and enhancement were observed for the poly(1-alkyne)[18b] and PPA[18a] systems, respectively.

The PL quenching can be ascribed to the electron and/or energy transfers from the excitons of the pyrenyl chromophores to the *l*-MWNT wires.[20a] However, the PL enhancement suggest that there is a competitive effect involved in the PPA system, which is helpful to the PL process. The incorporation of CNT may help enhance the PL efficiency through the reduction in the emission-quenching defects or exciton traps (e.g., radicals) in the PPA skeleton generated by photoexcitation.[34] When *l*-MWNT is added into the solution of P**1**, the favorable interactions between the *l*-MWNT walls and the PPA skeletons attract the polymer chains to wrap around the CNT surfaces.[18b] As a result, the fluorescence quenching defects or exciton traps in the PPA skeleton are annihilated by the radical capturing function of the CNT. This process decreases the likelihood of the exciton trapping by the PPA skeleton, thus promoting the radiative decay process. The Φ_F value is determined by the balance between the two competitive effects. Evidently, in the P**1**//*l*-MWNT system, the enhancement effect dominates, whereas in the P**2**//*l*-MWNT system, the quenching effect prevails.

Electrical Conductivity. The excellent solubility of the polymers and their hybrids with CNT have been confirmed by the usage of wet spectroscopic methods for their structure characterization as well as the solvating power evaluation discussed above. Using the solution-casting technique, smooth and homogeneous films are obtained from the solutions of P**1** and P**1**//*l*-MWNT hybrid (Figure 12). It should be stressed that the 1,2-dichloroethane solution of P**1**//*l*-MWNT was prepared by redissolving the dried hybrid powder. While many polymer/CNT hybrids reported so far become insoluble or partially insoluble after drying, our dried hybrids possess good redispersibility. The enhanced solubility, good redispersibility, and excellent film formability of the hybrid along with its unique functionalities pave the way to its potential applications in high-tech devices.

Table 2. X-ray Diffraction Analysis Data of P1, P2, and P1/*l*-MWNT[a]

sample	d_1[b]	d_2[b]	d_3[b]	d_4[b]	d_5[b]	d_6[b]	l[c]	phase
P1	20.62	4.35					38.09	SmA
P2	11.38	8.15	4.62	4.43	4.22	3.88	34.02	SmA
P1/*l*-MWNT	21.18	4.34					38.09	SmA

[a] The mesophases in the liquid crystal state at the given temperatures were frozen by the rapid quenching with liquid nitrogen. [b] Layer spacing (in units of Å). [c] Molecular length (in units of Å) calculated from the monomer repeat units in their fully extended conformation.

Chart 4

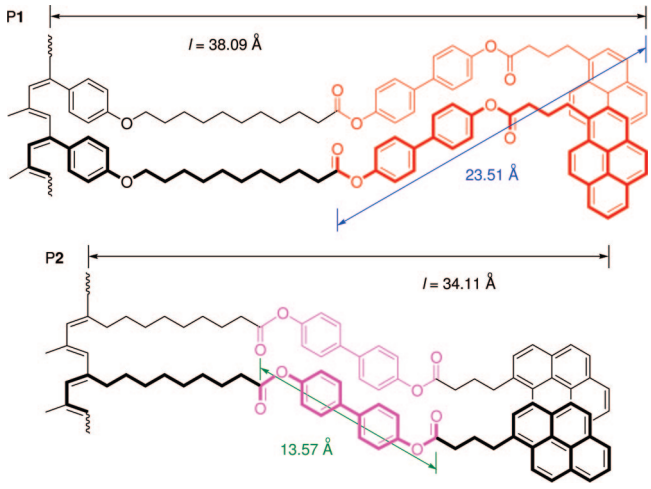

CNT is famous for its unique electrical properties,[36] and its hybrids with polymers have been found to show high conductivity.[37] Because of their high aspect ratio, the percolation thresholds in the CNT networks are one of the smallest among known materials.[37a,38] The attractive feature of the CNT-based hybrids is that the introduction of a relatively small amount of CNT can have a profound influence on the conductivity of the materials. Although the size-dependent liquid crystalline behaviors and the elasticity of CNT have been reported[39] and the thin films of the CNT-containing composites have been used as transparent conductive coatings,[37,38] the conductivity of the nanohybrids of CNT with liquid crystalline polymers has been rarely studied.

We measured the sheet resistivity (ρ_s) of the hybrid film by four-probe contact method based on the Hall effect. For comparison, the same test was carried out for polymer **P1**. The ρ_s value of **P1** could not be detected due to the detection limit of the apparatus, from which its resistivity is derived to be higher than 4×10^7 Ω/□. The sheet resistance of the **P1**/*l*-MWNT hybrid film at room temperature is merely 8720 Ω/□, indicative of a high electrical conductivity.

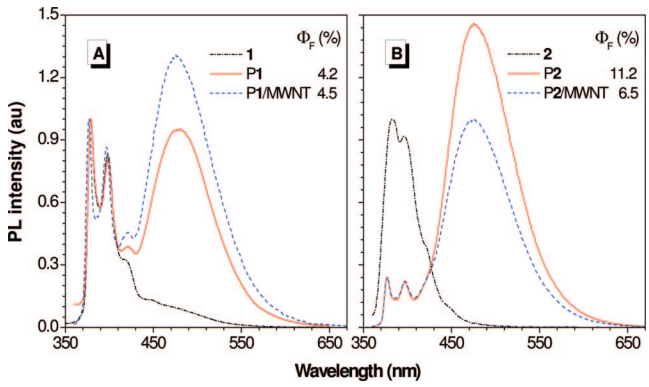

Figure 11. PL spectra of (A) **1**, **P1**, and **P1**/*l*-MWNT and (B) **2**, **P2**, and **P2**/*l*-MWNT in THF. Concentration (μM): 12.0 (for **1** and **P1**), 23.0 (for **2** and **P2**), 12.0 (for **P1** in **P1**/*l*-MWNT), 23.0 (for **P2** in **P2**/*l*-MWNT). Excitation wavelength: 343 nm. The fluorescence quantum yields were measured using the solutions with much lower concentrations (at absorbance <0.05).

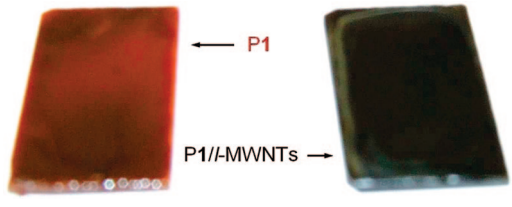

Figure 12. Photographs of (left) **P1** and (right) **P1**/*l*-MWNT films formed by casting their 1,2-dichloroethane solutions onto glass substrates.

Concluding Remarks

Functionalized polyacetylenes bearing biphenyl mesogens and pyrene or fluorene chromophores are successfully synthesized. Whereas none of their monomers are mesomorphic, **P1** and **P2** are liquid crystalline. The polymers are also light emitting. This work proves the feasibility of developing multifunctional polyacetylenes by melting various functional groups in one macromolecular structure. The difference in the mesomorphic behaviors between the monomers and polymers suggests that the polyacetylene chain has played a constructive role in the alignment and packing of the mesogenic units.

Insights into the structure−property relationships of the polymers are obtained in this study. Polymer **P1** shows higher solvating power to MWNT than **P2**, and the long-term stability of the solution of the **P1**/MWNT hybrid is better than that of its **P2**/MWNT counterpart, due to the synergistic and cooperative $\pi-\pi$ interactions of the multiple aromatic units in **P1** with the MWNT walls. Whereas the nanohybrids of MWNT with other polymers often become insoluble after drying, the dried hybrid powders of the nanohybrids developed in this work show good redispersibility and film formability.

Polymer **P2** is a better fluorophore than **P1** because of the exciton trapping effect of the PPA skeleton of the latter. The emission of **P2** in the **P2**/*l*-MWNT hybrid is attenuated because of the quenching effect of the MWNT. On the other hand, the PL efficiency of **P1** in the **P1**/*l*-MWNT nanohybrid is enhanced, thanks to the radical annihilation function of the MWNT. The films cast from the solutions of **P1** and its hybrid show sheet resistance of $>4 \times 10^7$ and 8720 Ω/□, respectively, indicating that the electrical conductivity of the nanohybrid is at least 4 orders of magnitude higher than that of its polymer parent. The multifunctional properties of the polyacetylenes and their hybrids make them promising for an array of technological applications.

Acknowledgment. The work reported in this paper was partially supported by the National Science Foundation of China (20634020 and 50573065), the Ministry of Science and Technology of China (2009CB623605), and the Research Grants Council of Hong Kong (603008 and 602706). B.Z.T. thanks the support from the Cao Guangbiao Foundation of Zhejiang University.

Supporting Information Available: Synthetic schemes, experimental procedures, and spectroscopic characterization data for the monomers and their polymers, IR and NMR spectra of **2** and **P2**, POM microphotographs of the monomers, absorption spectra

of the monomers, polymers, and hybrids, and absorption and emission spectra of **3** and P**3**. This material is free of charge via the Internet at http://pubs.acs.org.

References and Notes

(1) *Semiconducting Polymers: Chemistry, Physics and Engineering*, 1st ed.; Hadziioannou, G., van Hutten, P. F., Eds.; Wiley-VCH: Weinheim, Germany, 2000.

(2) (a) Burroughs, J. H.; Bradley, D. D. C.; Brown, A. B.; Marks, R. N.; Mackay, K.; Friend, R. H.; Burn, P. L.; Holmes, A. B. *Nature (London)* **1990**, *347*, 539. (b) Yu, W.-L.; Cao, Y.; Pei, J.; Huang, W.; Heeger, A. J. *Appl. Phys. Lett.* **1999**, *75*, 3270.

(3) Pei, Q.; Yu, G.; Zhang, C.; Yang, Y.; Heeger, A. J. *Science* **1995**, *269*, 1086.

(4) (a) Katz, H. E.; Bao, Z.; Gilat, S. L. *Acc. Chem. Res.* **2001**, *34*, 359. (b) Katz, H. E. *Chem. Mater.* **2004**, *16*, 4748.

(5) Samuel, I. D. W.; Turnbull, G. A. *Chem. Rev.* **2007**, *107*, 1272.

(6) (a) Alam, M. M.; Jenekhe, S. A. *Chem. Mater.* **2004**, *16*, 4647. (b) Coakley, K. M.; McGehee, M. D. *Chem. Mater.* **2004**, *16*, 4533.

(7) Dierking, I. *Adv. Mater.* **2000**, *12*, 167.

(8) (a) *Liquid-Crystalline Polymers*; Weiss, R. A., Ober, C. K., Eds.; American Chemical Society: Washington, DC, 1990. (b) *Liquid Crystalline Polymer Systems: Technological Advances*; Lsayev, A. I., Kyu, T., Cheng, S. Z. D., Eds.; American Chemical Society: Washington, DC, 1996. (c) *Optical Effects in Liquid Crystals*; Janossy, I., Ed.; Kluwer: Dordrecht, The Netherlands, 1991. (d) *An Introduction to Molecular Electronics*; Petty, M. C., Bryce, M. R., Bloor, D., Eds.; Edward Arnold: London, 1995.

(9) Lüssem. Festag, R.; Greiner, A.; Schmidt, C.; Unterlechner, C.; Heitz, W.; Wendorff, J. H.; Hopmeier, M.; Feldmann, J. *Adv. Mater.* **1995**, *7*, 923.

(10) Chen, S. H.; Conger, B. M.; Mastrangelo, J. C.; Kenda, A. S.; Kim, D. U. *Macromolecules* **1998**, *31*, 8051.

(11) Yoshino, K.; Yin, X. H.; Morita, S.; Nakazono, M.; Kawai, T.; Ozaki, M.; Jin, S. H.; Choi, S. K. *Jpn. J. Appl. Phys.* **1993**, *32*, L1673.

(12) Kawamoto, M.; Mochizuki, H.; Ikeda, T.; Iino, H.; Hanna, J. *J. Phys. Chem. B* **2005**, *109*, 9226.

(13) (a) Percec, V.; Asandei, A. D.; Hill, D. H.; Crawford, D. *Macromolecules* **1999**, *32*, 2597. (b) Chen, S. H.; Mastrangelo, J. C.; Conger, B. M.; Kende, A. D. *Macromolecules* **1998**, *31*, 3391. (c) Watanabe, Y.; Mihara, T.; Koide, N. *Macromol. Chem. Phys.* **1998**, *199*, 977. (d) Kijima, M.; Hasegawa, H.; Shirakawa, H. *J. Polym. Sci., Part A: Polym. Chem.* **1998**, *35*, 2691. (e) Gabaston,; L, I.; Foot, P. J. S.; Brown, J. W. *Chem. Commun* **1996**, 429. (f) Vincentini, F.; Barrceillet, J.; Laversanne, R.; Mauzac, M.; Bibonne, F.; Parneiz, J. P. *Liq. Cryst.* **1995**, *19*, 235. (g) Lieser, G.; Wegner, G. *Macromolecules* **1994**, *27*, 1027. (h) Thobie-Gauthier, C.; Bouligand, Y.; Gourges, A.; Jubault, M.; Roncali, J. *Adv. Mater.* **1994**, *6*, 138.

(14) (a) Lam, J. W. Y.; Tang, B. Z. *J. Polym. Sci., Part A: Polym. Chem.* **2003**, *41*, 2607. (b) Lam, J. W. Y.; Tang, B. Z. *Acc. Chem. Res.* **2005**, *38*, 745. (c) Yashima, E.; Maeda, K. *Macromolecules* **2008**, *41*, 3. (d) Masuda, T. *J. Polym. Sci., Part A: Polym. Chem.* **2007**, *45*, 165. (e) Tang, B. Z. *Macromol. Chem. Phys.* **2008**, *209*, 1303. (f) Li, C.; Li, Y. *Macromol. Chem. Phys.* **2008**, *209*, 1541. (g) Sanchez, J. C.; Trogler, W. C. *Macromol. Chem. Phys.* **2008**, *209*, 1527. (h) Rudick, J.; Percec, V. *Macromol. Chem. Phys.* **2008**, *209*, 1759. (i) Kwak, G.; Jin, S.-H.; Park, J.-W.; Gal, Y.-S. *Macromol. Chem. Phys.* **2008**, *209*, 1769. (j) Su, X. Y.; Xu, H. Y.; Guo, Q. Z.; Shi, G.; Yang, J. Y.; Song, Y. L.; Liu, X. Y. *J. Polym. Sci., Part A: Polym. Chem.* **2008**, *46*, 4529.

(15) (a) Tang, B. Z.; Kong, X.; Wan, X.; Feng, X.-D.; Kwok, H. S. *Macromolecules* **1998**, *31*, 2419. (b) Kong, X.; Lam, J. W. P.; Tang, B. Z. *Macromolecules* **1999**, *32*, 1722. (c) Lam, W. Y.; Dong, Y.; Cheuk, K. L.; Luo, J.; Kwok, H. S.; Tang, B. Z. *Macromolecules* **2002**, *35*, 1229. (d) Lam, W. Y.; Dong, Y.; Tang, B. Z. *Macromolecules* **2002**, *35*, 8288. (e) Lam, J. W. Y.; Qin, A.; Dong, Y.; Lai, L. M.; Häussler, M.; Dong, Y.; Tang, B. Z. *J. Phys. Chem. B* **2006**, *110*, 21613.

(16) Winnik, F. M. *Chem. Rev.* **1993**, *93*, 587.

(17) (a) Wang, Y.; Wang, H.; Liu, Y.; Di, C.; Sun, Y.; Wu, W.; Yu, G.; Zhang, D.; Zhu, D. *J. Am. Chem. Soc.* **2006**, *128*, 13058. (b) Strauss, J.; Daub, J. *Org. Lett.* **2002**, *4*, 683. (c) Lo, M. Y.; Zhen, C.; Lauters, M.; Jabbour, G. E.; Sellinger, A. *J. Am. Chem. Soc.* **2007**, *129*, 5808. (d) Kim, H. M.; Lee, Y. O.; Lim, C. S.; Kim, J. S.; Cho, B. R. *J. Org. Chem.* **2008**, *73*, 5127. (e) Zhu, H.; Lewis, F. D. *Bioconjugate Chem.* **2007**, *18*, 1213. (f) Lou, X.; Daussin, R.; Cuenot, S.; Duwez, A.-S.; Pagnoulle, C.; Detrembleur, C.; Bailly, C.; Jerome, R. *Chem. Mater.* **2004**, *16*, 4005.

(18) (a) Yuan, W.; Sun, J. Z.; Dong, Y.; Häussler, M.; Yang, F.; Xu, H. P.; Qin, A.; Lam, J. W. Y.; Zheng, Q.; Tang, B. Z. *Macromolecules* **2006**, *39*, 8011. (b) Yuan, W. Z.; Mao, Y.; Zhao, H.; Sun, J. Z.; Xu, H. P.; Jin, J. K.; Zheng, Q.; Tang, B. Z. *Macromolecules* **2008**, *41*, 701.

(19) (a) Winnik, M. A.; Bystryak, S. M.; Liu, Z. *Macromolecules* **1998**, *31*, 6855. (b) *Handbook of Fluorescence Spectra of Aromatic Molecules*; Berlman, I. B., Ed.; Academic Press: New York, 1971.

(20) (a) Guldi, D. M.; Rahman, G. M. A.; Zerbetto, F.; Prato, M. *Acc. Chem. Res.* **2005**, *38*, 871. (b) Tasis, D.; Tagmatarchis, N.; Georgakilas, V.; Prato, M. *Chem.—Eur. J.* **2003**, *9*, 4000. (c) Guldi, D. M.; Rahman, G. M. A.; Jux, N.; Balbinot, D.; Tagmatarchisc, N.; Prato, M. *Chem. Commun.* **2005**, 2038.

(21) (a) Sun, Y.-P.; Fu, K.; Lin, Y.; Huang, W. *Acc. Chem. Res.* **2002**, *35*, 1096. (b) Qu, L.; Martin, R. B.; Huang, W.; Fu, K.; Zweifel, D.; Lin, Y.; S.; un, Y. P.; Bunker, C. E.; Harruff, B. A.; Gord, R. D.; Allard, L. F. *J. Chem. Phys.* **2002**, *117*, 8089. (c) Bahun, G. J.; Wang, C.; Adronov, A. *J. Polym. Sci., Part A: Polym. Chem.* **2006**, *44*, 1941.

(22) (a) Tang, B. Z.; Xu, H. *Macromolecules* **1999**, *32*, 2569. (b) Li, Z.; Dong, Y.; Häussler, M.; Lam, J.W. Y.; Dong, Y.; Wu, L.; Wong, K. S.; Tang, B. Z. *J. Phys. Chem. B* **2006**, *110*, 2302. (c) Yuan, W. Z.; Sun, J. Z.; Liu, J. Z.; Dong, Y.; Li, Z.; Xu, H. P.; Qin, A. J.; Häussler, M.; Jin, J. K.; Zheng, Q.; Tang, B. Z. *J. Phys. Chem. B* **2008**, *112*, 8896. (d) Yuan, W. Z.; Zhao, H.; Xu, H. P.; Sun, J. Z.; Lam, J. W. Y.; Mao, Y.; Jin, J. K.; Zhang, S.; Zheng, Q.; Tang, B. Z. *Acta Polym. Sin.* **2007**, *10*, 901. (e) Zhao, H.; Yuan, W. Z.; Tang, L.; Sun, J. Z.; Xu, H. P.; Qin, A.; Mao, Y.; Jin, J. K.; Tang, B. Z. *Macromolecules* **2008**, *41*, 8566.

(23) Yuan, W. Z.; Tang, L.; Zhao, H.; Jin, J. K.; Sun, J. Z.; Qin, A.; Xu, H. P.; Liu, J.; Yang, F.; Zheng, Q.; Chen, E.; Tang, B. Z. *Macromolecules* **2009**, *42*, 52.

(24) (a) *Dictionary of Organometallic Compounds*, 2nd ed.; Chapman & Hall: London, 1995. (b) Schrock, R. R.; Osborn, J. A. *Inorg. Chem.* **1970**, *9*, 2339.

(25) Hirao, K.; Ishii, Y.; Terao, T.; Kishimoto, Y.; Miyatake, T.; Ikariya, T.; Noyori, R. *Macromolecules* **1998**, *31*, 3405.

(26) Kishimoto, Y.; Itou, M.; Miyatake, T.; Ikariya, T.; Noyori, R. *Macromolecules* **1995**, *28*, 6662.

(27) (a) Satake, A.; Miyajima, Y.; Kobuke, Y. *Chem. Mater.* **2005**, *17*, 716. (b) Ehli, C.; Rahman, G. M. A.; Jux, N.; Balbinot, D.; Guldi, D. M.; Paolucci, F.; Marcaccio, M.; Paolucci, D.; Melle-Franco, M.; Zerbetto, F.; Campidelli, S.; Prato, M. *J. Am. Chem. Soc.* **2006**, *128*, 11222. (c) Cheng, F.; Zhang, S.; Adronov, A.; Echegoyen, L.; Diederich, F. *Chem.—Eur. J.* **2006**, *12*, 6062.

(28) Masuda, T.; Tang, B. Z.; Higashimura, T.; Yamaoka, H. *Macromolecules* **1985**, *18*, 2369.

(29) Karim, S. M.; Nomura, R.; Masuda, T. *J. Polym. Sci., Part A: Polym. Chem.* **2001**, *39*, 3130.

(30) Brandrup, J., Immergut, E. H., Grulke, E. A., Eds.; *Polymer Handbook*, 4th ed.; Wiley: New York, 1999.

(31) (a) Lam, J. W. Y.; Kong, X.; Dong, Y.; Cheuk, K. K. L.; Xu, K.; Tang, B. Z. *Macromolecules* **2000**, *33*, 5027. (b) Lam, J. W. Y.; Dong, Y.; Cheuk, K. K. L.; Law, C. C. W.; Lai, L. M.; Tang, B. Z. *Macromolecules* **2004**, *37*, 6695.

(32) Kong, X.; Tang, B. Z. *Chem. Mater.* **1998**, *10*, 3352.

(33) Mariani, P.; Rustichelli, F.; Torquati, G. In *Physics of Liquid Crystalline Materials*; Khoo, I.-C., Simoni, F., Eds.; Gordon & Breach Science: New York, 1991; Chapter 1.

(34) Huang, Y. M.; Lam, J. W. Y.; Cheuk, K. K. L.; Ge, W.; Tang, B. Z. *Macromolecules* **1999**, *32*, 5976.

(35) Sanda, F.; Kawaguchi, T.; Masuda, T.; Kobayashi, N. *Macromolecules* **2003**, *36*, 2224.

(36) (a) Anantram, M. P.; Leonard, F. *Rep. Prog. Phys.* **2006**, *69*, 507. (b) Andrews, R.; Jacques, D.; Qian, D.; Rantell, T. *Acc. Chem. Res.* **2002**, *35*, 1008. (c) Ouyang, M.; Huang, J.-L.; Lieber, C. M. *Acc. Chem. Res.* **2002**, *35*, 1018. (d) Avouris, P. *Acc. Chem. Res.* **2002**, *35*, 1026. (e) Dai, H. *Acc. Chem. Res.* **2002**, *35*, 1035.

(37) (a) Fujigaya, T.; Haraguchi, S.; Fukumaru, T.; Nakashima, N. *Adv. Mater.* **2008**, *20*, 2151. (b) Blackburn, J. L.; Barnes, T. M.; Beard, M. C.; Kim, Y. H.; Tenent, R. C.; McDonald, J.; To, B.; Coutts, T. J.; Heben, M. J. *ACS Nano* **2008**, *2*, 1266. (c) Green, A. A.; Hersam, M. C. *Nano Lett.* **2008**, *14*, 1417. (d) Kim, S. N.; Rusling, J. F.; Papadimitrakopoulos, F. *Adv. Mater.* **2007**, *19*, 3214. (e) Fukushima, T.; Kosaka, A.; Yamamoto, Y.; Aimiya, T.; Notazawa, S.; Takigawa, T.; Inabe, T.; Aida, T. *Small* **2006**, *2*, 554. (f) Hinds, B. J.; Chopra, N.; Rantell, T.; Andrews, R.; Gavalas, V.; Bachas, L. G. *Science* **2004**, *303*, 62.

(38) (a) Behnam, A.; Guo, J.; Ural, A. *J. Appl. Phys.* **2007**, *102*, 044313–1. (b) Kacabas, C.; Pimparkar, N.; Yesilyurt, O.; Kang, S. J.; Alam, M. A.; Rogers, J. A. *Nano Lett.* **2007**, *7*, 1195. (c) Li, J.; Ma, P. C.; Chow, W. S.; To, C. K.; Tang, B. Z.; Kim, J. K. *Adv. Funct. Mater.* **2007**, *17*, 3207. (d) Unalan, H. E.; Fanchini, G.; Kanwal, A.; Du Pasquier, A.; Chhowalla, M. *Nano Lett.* **2006**, *6*, 677. (e) Kumar, S.; Murthy, J. Y.; Alam, M. A. *Phys. Rev. Lett.* **2005**, *95*, 066802–1.

(39) Song, W.; Windle, A. H. *Adv. Mater.* **2008**, *20*, 3149.

MA802510E